

Dark matter transient annihilations in the early Universe

Katsuya Hashino,^{1,*} Jia Liu,^{2,1,†} Xiao-Ping Wang,^{3,4,‡} and Ke-Pan Xie^{5,§}

¹Center for High Energy Physics, Peking University, Beijing 100871, China

²School of Physics and State Key Laboratory of Nuclear Physics and Technology, Peking University, Beijing 100871, China

³School of Physics, Beihang University, Beijing 100083, China

⁴Beijing Key Laboratory of Advanced Nuclear Materials and Physics, Beihang University, Beijing 100191, China

⁵Department of Physics and Astronomy, University of Nebraska, Lincoln, NE 68588, USA

The cosmological evolution can modify the dark matter (DM) properties in the early Universe to be vastly different from the properties today. Therefore, the relation between the relic abundance and the DM constraints today needs to be revisited. We propose novel *transient* annihilations of DM which helps to alleviate the pressure from DM null detection results. As a concrete example, we consider the vector portal DM and focus on the mass evolution of the dark photon. When the Universe cools down, the gauge boson mass can increase monotonically and go across several important thresholds; opening new transient annihilation channels in the early Universe. Those channels are either forbidden or weakened at the late Universe which helps to evade the indirect searches. In particular, the transient resonant channel can survive direct detection (DD) without tuning the DM to be half of the dark photon mass and can be soon tested by future DD or collider experiments. A feature of the scenario is the existence of a light dark scalar.

I. INTRODUCTION

The Weakly Interacting Massive Particle (WIMP) paradigm provides an elegant explanation to dark matter (DM) via the freeze-out mechanism. It suggests that the DM particle has weak scale couplings to the Standard Model (SM) particles. This implies sizable scattering rates between local DM and nucleons [1–4], residual DM annihilation today in galaxies [5–9], and DM production at colliders [10–13]. However, the null results from the above experiments cast doubt on the WIMP paradigm.

One of the most common benchmark WIMP model is the vector portal DM; in which the DM fermion ψ interacts with the SM particles through kinetic mixing of the $U(1)_d$ dark photon A' and SM photon [14]. The ratio $r_0 \equiv m_{A'}/m_\psi$ classifies the parameter space into different regions. For $r_0 < 1$, the classic secluded annihilation to dark photon pair is kinematically allowed [15]. For $1 \lesssim r_0 \lesssim 2$, there are new channels allowing secluded annihilations [16–20]. For $r_0 > 2$, the DM pair will annihilate into SM particles through s -channel A' mediation; thus, there is a direct connection between the relic abundance and nucleon scattering cross-section. For DM mass > 10 GeV, most of the parameter space is already ruled out by direct detection (DD). The exception being the cases of $r_0 \approx 2$ (the fine-tuned s -channel resonant region) or inelastic DM (with small mass splitting) [21–29]. Light DM can avoid DD, but is still subject to constraints from cosmic microwave background (CMB) measurements [21, 30] and the intensity frontier experiments [24, 25]. Therefore, the vector portal DM model is severely constrained by the experiments.

In this *Letter*, we point out that the DM evolution can be deeply affected by the thermal history of the Universe; hence, the above constraints cannot be trivially applied. More specifically, the $U(1)_d$ is restored when the cosmic temperature is very high. If the $U(1)_d$ breaking is through a second-order phase transition, then, as the Universe cools down, the A' mass will scan from zero to today's zero temperature value. For $r_0 > 2$, such a “mass scanning” will open transient secluded annihilations and s -channel resonant annihilation which help evade current DD, indirect detection, and collider searches. This scenario is testable by near future DM experiments and can serve as a viable variant of the WIMP model.

There have been prior studies on the effects cosmological evolution have on DM or scalar mediator mass, stability, interaction couplings, and annihilation channels [31–47]. In our scenario, we, for the first time, focus on the vector mediator whose mass is significantly affected during the freeze-out. The DM mass and its couplings are not affected at the freeze-out temperature. Moreover, the Higgs boson responsible for the $U(1)_d$ breaking has to be much lighter than A' ; a feature of this scenario.

II. MODEL

The vector portal DM model has the following Lagrangian

$$\mathcal{L}_d = \bar{\psi} (i\not{D} - m_\psi) \psi - \frac{1}{4} F'_{\mu\nu} F'^{\mu\nu} + \epsilon e A'_\mu J_{\text{em}}^\mu, \quad (1)$$

where $D_\mu \equiv \partial_\mu - ig_d A'$, and J_{em}^μ is the SM electromagnetic current. The coupling between J_{em}^μ and A' comes from the kinetic mixing with the photon field strength. The $U(1)_d$ is spontaneously broken by a complex scalar $\Phi = (\phi + i\eta)/\sqrt{2}$ with the potential

$$V(\Phi) = \mu_d^2 |\Phi|^2 + \lambda_d |\Phi|^4. \quad (2)$$

* hashino@pku.edu.cn

† jialiu@pku.edu.cn

‡ hcwangxiaoping@buaa.edu.cn

§ kepan.xie@unl.edu

Provided that $\mu_d^2 < 0$, the scalar field obtains a vacuum expectation value (VEV) $\langle \phi \rangle = v_d \equiv \sqrt{-\mu_d^2/\lambda_d}$, and hence, A' acquires a mass $m_{A'} = g_d v_d$. The real part of the scalar ϕ also obtains a mass $m_\phi = \sqrt{2\lambda_d} v_d$.

The scalar potential in Eq. (2) receives corrections in the early Universe. For example, if there is a light scalar S coupling to Φ via $\lambda_{\phi S} |\Phi|^2 S^2$, a thermal mass term $\lambda_{\phi S} T^2 \phi^2/12$ can be induced. Another possible correction comes from the gravitational coupling $\xi_\phi R |\Phi|^2/2$, where R is the Ricci curvature scalar. As $R/H^2 \sim 10^{-2}-10^{-1}$ at temperature between 100 MeV and 10 GeV (with H being the Hubble constant) [47–49], the portal coupling provides a T^4 correction to the scalar mass term. Moreover, corrections like $m_* H \Phi^2$ or $H^2 \Phi^2$ can also arise from the flat directions in supersymmetric models [50, 51]. In general, the potential in the early Universe can be written as

$$\mu_d^2(T) = \mu_{d,0}^2 + c_\phi T^n, \quad (3)$$

where the dimension of the coefficient c_ϕ is $[\text{Energy}^{(2-n)}]$ with $n = 2$ or 4 . The scalar VEV varies with the temperature as,

$$v_d^2(T) = \begin{cases} 0 & T > T_\phi \\ v_{d,0}^2 - c_\phi T^n / \lambda_d & T < T_\phi \end{cases}, \quad (4)$$

where $T_\phi = (\lambda_d v_{d,0}^2 / c_\phi)^{1/n}$ is a temperature at which the second-order phase transition for $U(1)_d$ breaking starts. The evolution of $m_{A'}$ can be derived immediately, i.e.,

$$m_{A'}^2(T) = \begin{cases} 0 & T > T_\phi \\ m_{A',0}^2 - \kappa m_\psi^2 \left(\frac{T}{m_\psi}\right)^n & T < T_\phi \end{cases}, \quad (5)$$

where $m_{A',0} = g_d v_{d,0}$ is the mass at zero temperature and $\kappa = m_\psi^{n-2} c_\phi g_d^2 / \lambda_d$ is a model dependent dimensionless constant. Later, we will see that κ is required to be large.

The mass of ϕ is also temperature-dependent,

$$m_\phi^2(T) = \begin{cases} \mu_d^2 + c_\phi T^n & T > T_\phi \\ m_{A'}^2(T) \times \left(2m_\psi^{n-2} c_\phi / \kappa\right) & T < T_\phi \end{cases}. \quad (6)$$

Since κ is large, a scalar ϕ much lighter than A' is a feature of our model. More specifically, for $n = 2$, we are interested in $\kappa \sim 10^4$ with $c_\phi \sim 1/12$, and hence, the mass of ϕ is sub-GeV. To avoid constraints from cosmological observations, a small Higgs portal coupling $\lambda_{h\phi} |H|^2 |\Phi|^2$ is assumed to allow ϕ to decay to a pair of SM light fermions before Big Bang nucleosynthesis. For $n = 4$, since $c_\phi \sim 1/m_{\text{pl}}^2$, with $m_{\text{pl}} = 1.22 \times 10^{19}$ GeV being the Planck scale, a very small $\lambda_d \sim 10^{-38}$ is required for $T_\phi \sim 1$ GeV. Hence, an extremely light ϕ with $m_\phi \sim \mathcal{O}(10^{-10}$ eV) exists. The smallness of λ_d , or in other words, the flatness of the potential Eq. (2) can be achieved by embedding the model into either a spontaneously broken global symmetry with Φ

as the pseudo-Nambu-Goldstone boson or a supersymmetric model with Φ as the moduli field.

In summary, the cosmological evolution effects on A' is fully encoded in the constant κ . This serves as an extra free parameter compared to the zero temperature model. Therefore, there are five input parameters in total,

$$\{m_\psi, m_{A',0}, g_d, \epsilon, \kappa\}. \quad (7)$$

For convenience, we drop the (T) for the explicit temperature dependence thereafter, e.g., $m_{A'}$ always implies $m_{A'}(T)$. The subscript “0” denotes the zero temperature values.

III. TRANSIENT ANNIHILATIONS

For $r_0 = m_{A',0}/m_\psi > 2$, as the temperature drops, $m_{A'}$ will inevitably go across several thresholds:

$$\begin{aligned} \text{Transient secluded: } & (A'A') \quad m_{A'} = m_\psi, \\ & (A'\phi) \quad m_{A'} = 2m_\psi - m_\phi, \\ \text{Transient resonant: } & (\bar{f}f) \quad m_{A'} = 2m_\psi. \end{aligned} \quad (8)$$

Crossing the first two thresholds open up new transient annihilation channels $\bar{\psi}\psi \rightarrow A'A'$ and $\bar{\psi}\psi \rightarrow A'\phi$. These are secluded annihilation and thus, can evade the DD limits and the collider constraints. The last crossover enables a transient s -channel resonance, $\bar{\psi}\psi \rightarrow A' \rightarrow \bar{f}f$, which greatly enhances the annihilation cross-section. Defining $x \equiv m_\psi/T$, we denote those temperatures as $x_{A'A'}$, $x_{A'\phi}$ and x_{res} respectively. If they happen to be around the freeze-out temperature $x_{\text{fo}} \sim 23$, the relic abundance calculation has to incorporate those transient annihilations. This coincidence generally requires a large $\kappa \gtrsim x_{\text{fo}}^n (r_0^2 - a)$, with $a = 1$ (4) for $A'A'$ ($\bar{f}f$) final states respectively.

The relevant annihilation cross-sections are

$$\langle \sigma v_{A'A'} \rangle \approx \frac{g_d^4}{16\pi m_\psi^2} (1-r^2)^{3/2} (1-r^2/2)^{-2}, \quad (9)$$

$$\langle \sigma v_{A'\phi} \rangle \approx \frac{g_d^4}{256\pi m_\psi^2} \frac{r^4 + 40r^2 + 16}{|4-r^2|} + \mathcal{O}\left(\frac{m_\phi^2}{m_{A'}^2}\right), \quad (10)$$

$$\langle \sigma v_{\bar{f}f} \rangle = \frac{g_d^2 \epsilon^2 e^2}{6\pi} \frac{s + 2m_\psi^2}{(s - m_{A'}^2)^2 + m_{A'}^2 \Gamma_{A'}^2}, \quad (11)$$

where $r \equiv m_{A'}/m_\psi$, s is the total energy square in the center of mass frame and $\Gamma_{A'}$ is the decay width for A' which is also temperature dependent.

For the *transient secluded* channels ($A'A'$ and $A'\phi$), we approximate their thermally averaged values as the s -wave part of their cross-section. The cosmological evolution effects on $m_{A'}$ is not affected by this approximation as the thermal average is taken over the DM velocity distribution. For $\langle \sigma v_{A'\phi} \rangle$, the above is obtained by expanding over small m_ϕ and is used in the analytic relic abundance calculation. The full expression is given in the

Appendix and is applied in the numeric calculation. This channel has an accidental resonant enhancement due to small m_ϕ , but never hits the resonant peak. This occurs near $x_{A'\phi}$, when the factor $|4-r^2|^{-1}$ becomes $m_\psi/(4m_\phi)$ at the leading order. Due to this enhancement, the annihilation channel $A'\phi$ dominates over $A'A'$ most of the time.

For the *transient resonant* channel ($\bar{f}f$), one generally performs the thermal average numerically. However, to understand the transient resonant annihilation better, we simplify its expression for the analytic relic abundance calculation. For narrow width resonances, the resonance peak of Eq. (11) can be approximated by a δ -function. This leads to the following expression for the thermally averaged cross-section,

$$\langle\sigma v\rangle_{\bar{f}f}^{\text{res}} \approx \frac{g_d^2 \epsilon^2 e^2 (2+r^2)x}{48\sqrt{2\pi}m_\psi\Gamma_{A'}} \sqrt{r(r^2-4)}x e^{-(r-2)x}. \quad (12)$$

This is valid for $x > x_{\text{res}} = (\kappa/(r_0^2-4))^{1/n}$ with resonance at $m_{A'}|_{x_{\text{res}}} = 2m_\psi$. The width of A' can be approximated as

$$\Gamma_{A'} \approx \frac{m_{A'}}{12\pi} \left[\epsilon^2 e^2 n_{\text{dof}} + g_d^2 \sqrt{1 - \frac{4}{r^2}} \left(1 + \frac{2}{r^2}\right) \right], \quad (13)$$

where $n_{\text{dof}} \equiv \sum_f Q_f^2 N_f^c = 20/3$ with charge Q_f and color factor N_f^c , summed over SM fermions lighter than the top quark. We neglect the SM fermion masses to further simplify the decay width. In the small g_d regime, $g_d \lesssim \sqrt{n_{\text{dof}}}\epsilon e$, the decay width is dominated by the SM contribution and the cross-section $\langle\sigma v\rangle_{\bar{f}f}^{\text{res}}$ will be proportional to g_d^2 . While if $g_d \gtrsim \sqrt{n_{\text{dof}}}\epsilon e$, the width is controlled by the invisible decay to $\psi\psi$ and the cross-section $\langle\sigma v\rangle_{\bar{f}f}^{\text{res}}$ will be proportional to $\epsilon^2 e^2$. However, in the large g_d case, the contribution from transient secluded channels dominates the DM evolution. Therefore, small g_d is more interesting for transient resonant annihilation.

The cross-section $\langle\sigma v\rangle_{\bar{f}f}^{\text{res}}$ has an exponential penalty factor from Boltzmann suppression but is unsuppressed near the resonance. The cross-section can be greatly simplified by taking $x = x_{\text{res}} + \Delta x$ and expanding to leading order in $\Delta x \ll 1$. An important step is keeping the exponential term; otherwise, the Boltzmann suppression vanishes. In this limit, we have

$$\sum_f \langle\sigma v\rangle_{\bar{f}f}^{\text{res}} \approx \frac{3\sqrt{n\pi}\Delta x g_d^2}{4m_\psi^2} e^{-\frac{n\Delta x}{4}(r_0^2-4)} \times (r_0^2-4)^{\frac{n-2}{2n}} \kappa^{1/n} + \mathcal{O}(g_d^4\Delta x), \quad (14)$$

where the expansion of small Δx also implicitly requires small g_d , i.e., $g_d \lesssim \sqrt{n_{\text{dof}}}\epsilon e$. At leading order, we see the cross-section increases with $\kappa^{1/n} g_d^2$. In the Appendix, we give the next order term and show that the analytic results for $\langle\sigma v\rangle$ are in consonance with numeric calculations for all three channels.

IV. RELIC ABUNDANCE

The DM relic abundance can be obtained by solving the Boltzmann equation. Using the DM yield $Y \equiv n_\psi/s$, with s being the entropy density, one can reformulate the equation as

$$\frac{dY}{dx} = -\sqrt{\frac{\pi g_*}{45}} \frac{m_{\text{pl}} m_\psi}{x^2} \langle\sigma v\rangle (Y^2 - Y_{\text{eq}}^2), \quad (15)$$

where g_* is the number of effective degree of freedom and Y_{eq} is the yield at equilibrium. The thermally averaged cross-section $\langle\sigma v\rangle$ includes all DM annihilation channels. The DM relic abundance can be computed numerically; noting that $m_{A'}$ and m_ϕ will change with x .

Furthermore, the relic abundance can be computed analytically as

$$Y^{-1}(x = \infty) \approx \int_{x_{\text{fo}}}^{\infty} dx \sqrt{\frac{\pi g_*}{45}} \frac{m_{\text{pl}} m_\psi}{x^2} \langle\sigma v\rangle, \quad (16)$$

where we have used the approximations that when freeze-out starts, $Y \gg Y_{\text{eq}}$ and $Y(x_{\text{fo}}) \gg Y(x = \infty) \equiv Y_0$.

Therefore, the annihilation contribution from $A'A'$ can be obtained by plugging in Eq. (9),

$$Y_{A'A'}^{-1} = \frac{g_d^4 g_*^{1/2} m_{\text{pl}}}{48\sqrt{5\pi}m_\psi} F_{A'A'}(x, r_0, \kappa) \Big|_{x_{\text{fo}}}^{x_{A'A'}}, \quad (17)$$

where $F_{A'A'}$ is an indefinite integration function, which is given in the Appendix. Similarly, we obtain the yield inverse $Y_{A'\phi}^{-1}$ using the simplified thermally averaged cross-section in Eq. (10),

$$Y_{A'\phi}^{-1} = \sqrt{\frac{g_*}{5\pi}} \frac{g_d^4 m_{\text{pl}}}{768m_\psi} F_{A'\phi}(x, r_0, \kappa) \Big|_{x_{\text{fo}}}^{x_{A'\phi}}, \quad (18)$$

where the indefinite integration function $F_{A'\phi}$ can be found in the Appendix.

For the resonant channel $\bar{f}f$, using the simplified resonant cross-section Eq. (14), one can find

$$Y_{\text{res}}^{-1} \approx \sqrt{\frac{\pi^3 g_*}{5}} \frac{g_d^2 m_{\text{pl}}}{nm_\psi} (r_0^2-4)^{\frac{1-n}{n}} \kappa^{-1/n} \times \left(1 - \frac{3g_d^2(r_0^2-4)^{1/(2n)}}{\sqrt{\pi}n_{\text{dof}}\epsilon^2 e^2} \kappa^{-1/(2n)}\right), \quad (19)$$

where the second term in the bracket comes from the A' decay to DM pair. For different n , one can choose a κ to get the same relic abundance. For example, when switching from $n = 2$ to $n = 4$, one can rescale $\kappa \rightarrow \kappa^2/(16(r_0^2-4))$ to obtain similar Y_{res} .

Now we show the numerical results. In Fig. 1, we show the required g_d to obtain the correct relic abundance for each individual annihilation channel $A'A'$, $A'\phi$ and $\bar{f}f$ with $n = 2$. The dashed and solid lines are from analytic and numeric calculations for Y^{-1} respectively. They are in good agreement with each other. We see that the

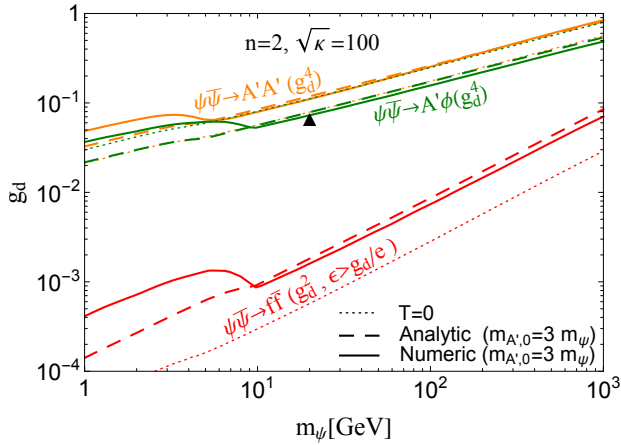


Figure 1. g_d as a function of m_ψ for transient annihilation channels $A'A'$, $A'\phi$ and $\bar{f}f$, which provides the right relic abundance for $n = 2$. The dashed and solid lines are analytic and numeric calculations respectively. We also compare them with a set of zero temperature examples (dotted lines) described in the text. The benchmark \blacktriangle has included the contribution from both $A'A'$ and $A'\phi$, and will be described in Fig. 2.

required g_d for $\bar{f}f$ is much smaller than $A'A'$ and $A'\phi$. This is because the s -channel resonant enhancement Y_{res}^{-1} is proportional to g_d^2 . By contrast, for $A'A'$ and $A'\phi$, their Y^{-1} are both proportional to g_d^4 and do not depend on ϵ . The required g_d for $A'\phi$ is smaller than $A'A'$ due to the accidental resonant enhancement factor $m_\psi/m_\phi \gg 1$.

In Fig. 1, we also compare our transient results with zero temperature examples labeled as $T = 0$ and drawn with thin dotted lines. For $A'A'$ and $A'\phi$ channels, we force A' and ϕ to be massless. Unsurprisingly, the required g_d is smaller for $T = 0$ compared with transient annihilation for $A'A'$ channel. However, for $A'\phi$, the required g_d increased for $T = 0$ since there is no accidental resonant enhancement. For $\bar{f}f$, we take the fine-tuned resonant example with $m_{A',0} = 2m_\psi$. The required g_d decreases by a factor of a few as expected.

In Fig. 2, we plot Y as a function of x and show the evolution with all annihilation channels included. For the upper panel, it shows that the contribution from transient secluded annihilation $A'A'$ and $A'\phi$ dominates with large g_d and can lead to the correct relic abundance. For the lower panel, the transient resonant annihilation $\bar{f}f$ dominates with small g_d . We show the two benchmarks with (without) cosmological evolution effects using $\sqrt{\kappa} = 100$ (0). Without evolution effects, the transient secluded channels are kinematically forbidden.

V. CONSTRAINTS

For transient secluded annihilations $A'A'$ and $A'\phi$, the collider and DD bounds can be easily evaded by choos-

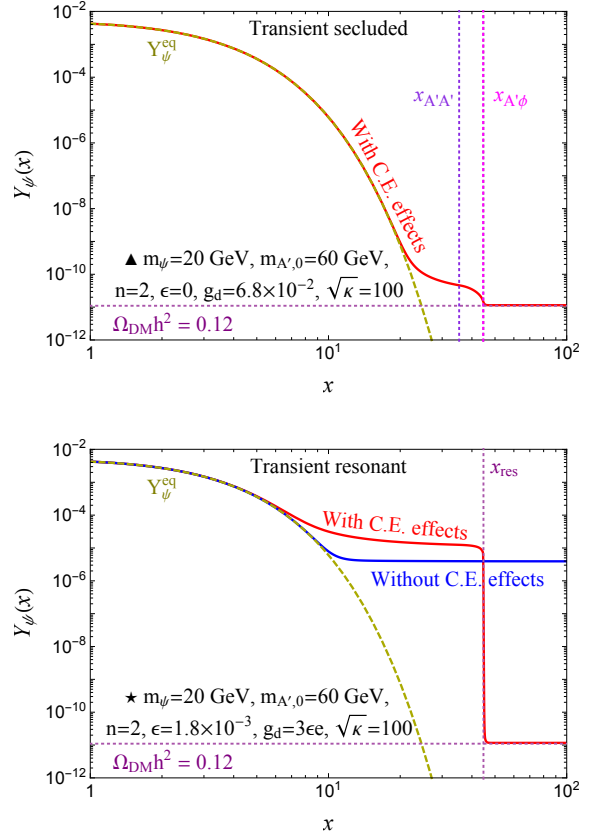


Figure 2. The DM yield Y as a function of x for all the transient annihilation channels $A'A'$, $A'\phi$ and $\bar{f}f$ included. Two benchmarks with large (\blacktriangle) and small (\star) g_d are shown respectively in the upper and lower panels for $n = 2$. For the lower panel, the Y 's with and without cosmological evolution (C.E.) effects are both shown for comparison.

ing a tiny ϵ . However, it does not work for the transient resonant annihilation $\bar{f}f$. This is because its annihilation cross-section will be proportional to ϵ^2 in the small ϵ limit, making the cross-section not large enough to provide the right relic abundance. Therefore, we choose a moderate ϵ satisfying $g_d \lesssim \sqrt{n_{\text{dof}}}\epsilon$. Hence, the annihilation cross-section is still proportional to g_d^2 . We consider the constraints from DD bounds [3, 4] and dilepton and mono-photon searches at colliders [52–57]. Since the transient annihilations are either forbidden or weakened in the late universe, the indirect detection does not constrain the scenario in general. For example, the transient resonant benchmark has annihilation cross-section of about $10^{-34}\text{cm}^3/\text{s}$ at the CMB era which is much smaller than the CMB and indirect search bounds.

The nucleon scattering cross-section is given as,

$$\sigma_p^{\text{SI}} = \frac{\epsilon^2 e^2 g_d^2}{\pi} \frac{\mu_{\psi p}^2}{m_{A',0}^4}, \quad (20)$$

with reduced mass $\mu_{\psi p} \equiv m_\psi m_p / (m_\psi + m_p)$. Since the resonant cross-section is proportional to $g_d^2 \epsilon^2 e^2 / (g_d^2 +$

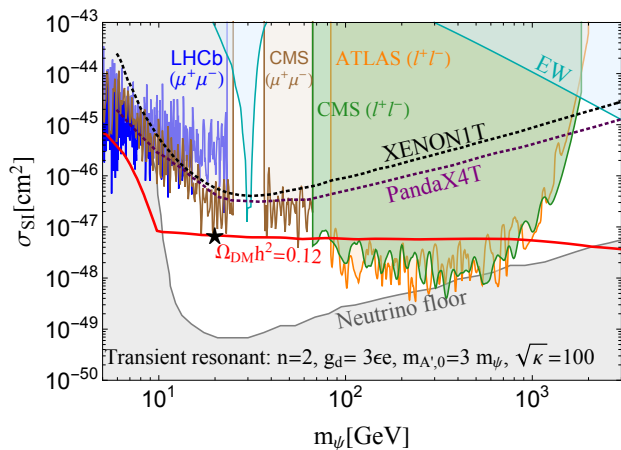


Figure 3. The constraints for transient s -channel resonance model from DD [3, 4] and dilepton searches at LHC [55–58]. We choose optimal $g_d = 3\epsilon e$ to evade the existing limits and fix the mass ratio $m_{A',0} = 3m_\psi$ and $\sqrt{\kappa} = 100$. The benchmark \star of Fig. 2 is also displayed.

$n_{\text{dof}}\epsilon^2 e^2$) and the nucleon scattering cross-section is proportional to $g_d^2\epsilon^2 e^2$, there is an optimal point around $g_d \approx \sqrt{n_{\text{dof}}\epsilon e}$ yielding a small DD signal for a given DM relic abundance. We choose this point as our benchmark \star in Fig. 2.

In Fig. 3, we show the DD and collider constraints for transient resonant annihilation and compare them with the relic abundance requirement. The only free parameters are ϵ and m_ψ . The others are fixed by the relations $m_{A',0} = 3m_\psi$, $g_d = 3\epsilon e$ and $\sqrt{\kappa} = 100$ for $n = 2$. The signal shown in red becomes flat for $m_\psi > 10$ GeV because the relic abundance requires g_d^2/m_ψ^2 to be roughly constant while σ_{SI} is proportional to g_d^4/m_ψ^4 in this setup.

We can see that the transient resonant annihilation helps to evade the current DD limits from XENON1T and PandaX-4T even for $m_\psi \neq m_{A',0}/2$. Moreover, it is well within the reach of future experiments and can be soon tested before reaching the neutrino floor. The dilepton searches from LHCb [55], CMS [56, 58] and ATLAS [57] are most relevant and stringent; even with significant invisible decay branching ratio $A' \rightarrow \bar{\psi}\psi$. The ATLAS and CMS results leave two windows for DM mass within 10–100 GeV and $\gtrsim 1$ TeV. Besides the benchmark, taking a smaller $g_d/(\epsilon e)$ ratio will not help. With the required g_d

from the relic abundance, ϵ is not small enough to evade DD and dilepton searches. On the other hand, choosing a large $g_d/(\epsilon e)$ ratio does not work either. The required g_d for the relic abundance increases significantly; thus, ϵ is still too large. Taking a smaller mass ratio $r_0 \rightarrow 2$ will definitely help as shown in the $T = 0$ example in Fig. 1. This significantly decreases g_d ; thus, alleviates the tension from ϵ . Therefore, the parameter space for the transient resonant annihilation is pretty restricted and future collider and DD searches can soon fully test it.

VI. CONCLUSION

We studied the effects of cosmological evolution on DM annihilation in the early Universe; especially for the gauge boson mediator. They can open new transient secluded and resonant annihilation channels which change the experimental constraints on the model parameter space. We have obtained the analytic forms of the relic abundance for each transient annihilation and they are in good agreement with full numeric calculations. We choose $r_0 > 2$ as an example for all three channels. The transient secluded annihilations become fully secluded; with no DD and collider signal and even negligible indirect detection signal. The transient resonant annihilation is a viable and promising WIMP variant. It can evade the current DD and dilepton searches and can be fully tested by experiments in the near future. There are two windows opening for DM mass within 10–100 GeV and around 1 TeV. If $r_0 \rightarrow 2$, there are more parameter space opens for transient resonant annihilation. For $1 < r_0 < 2$, the transient annihilations are still viable and important. The dark Higgs has to be much lighter than the gauge boson, which is a feature of the transient annihilation scenario.

ACKNOWLEDGMENTS

The authors would like to thank Chengcheng Han, Joachim Kopp, Lu Yin for helpful discussions, and Wen Han Chiu for proofreading. The work of JL is supported by National Science Foundation of China under Grant No. 12075005 and by Peking University under startup Grant No. 7101502458. The work of XPW is supported by National Science Foundation of China under Grant No. 12005009. KPX is supported by the University of Nebraska-Lincoln.

-
- [1] **LUX** Collaboration, D. S. Akerib *et al.*, “Results from a search for dark matter in the complete LUX exposure,” *Phys. Rev. Lett.* **118** no. 2, (2017) 021303, [arXiv:1608.07648](https://arxiv.org/abs/1608.07648) [[astro-ph.CO](https://arxiv.org/abs/1608.07648)].
- [2] **CDEX** Collaboration, Z. Z. Liu *et al.*, “Constraints on Spin-Independent Nucleus Scattering with sub-GeV

- Weakly Interacting Massive Particle Dark Matter from the CDEX-1B Experiment at the China Jinping Underground Laboratory,” *Phys. Rev. Lett.* **123** no. 16, (2019) 161301, [arXiv:1905.00354](https://arxiv.org/abs/1905.00354) [[hep-ex](https://arxiv.org/abs/1905.00354)].
- [3] **XENON** Collaboration, E. Aprile *et al.*, “Dark Matter Search Results from a One Ton-Year Exposure of

- XENON1T,” *Phys. Rev. Lett.* **121** no. 11, (2018) 111302, [arXiv:1805.12562 \[astro-ph.CO\]](#).
- [4] **PandaX** Collaboration, Y. Meng et al., “Dark Matter Search Results from the PandaX-4T Commissioning Run,” [arXiv:2107.13438 \[hep-ex\]](#).
- [5] **AMS** Collaboration, M. Aguilar et al., “Electron and Positron Fluxes in Primary Cosmic Rays Measured with the Alpha Magnetic Spectrometer on the International Space Station,” *Phys. Rev. Lett.* **113** (2014) 121102.
- [6] **AMS** Collaboration, L. Accardo et al., “High Statistics Measurement of the Positron Fraction in Primary Cosmic Rays of 0.5–500 GeV with the Alpha Magnetic Spectrometer on the International Space Station,” *Phys. Rev. Lett.* **113** (2014) 121101.
- [7] **Fermi-LAT** Collaboration, M. Ackermann et al., “Searching for Dark Matter Annihilation from Milky Way Dwarf Spheroidal Galaxies with Six Years of Fermi Large Area Telescope Data,” *Phys. Rev. Lett.* **115** no. 23, (2015) 231301, [arXiv:1503.02641 \[astro-ph.HE\]](#).
- [8] **Fermi-LAT, DES** Collaboration, A. Albert et al., “Searching for Dark Matter Annihilation in Recently Discovered Milky Way Satellites with Fermi-LAT,” *Astrophys. J.* **834** no. 2, (2017) 110, [arXiv:1611.03184 \[astro-ph.HE\]](#).
- [9] **DAMPE** Collaboration, G. Ambrosi et al., “Direct detection of a break in the teraelectronvolt cosmic-ray spectrum of electrons and positrons,” *Nature* **552** (2017) 63–66, [arXiv:1711.10981 \[astro-ph.HE\]](#).
- [10] **CMS** Collaboration, A. M. Sirunyan et al., “Search for invisible decays of a Higgs boson produced through vector boson fusion in proton-proton collisions at $\sqrt{s} = 13$ TeV,” *Phys. Lett. B* **793** (2019) 520–551, [arXiv:1809.05937 \[hep-ex\]](#).
- [11] **ATLAS** Collaboration, M. Aaboud et al., “Combination of searches for invisible Higgs boson decays with the ATLAS experiment,” *Phys. Rev. Lett.* **122** no. 23, (2019) 231801, [arXiv:1904.05105 \[hep-ex\]](#).
- [12] **ATLAS** Collaboration, G. Aad et al., “Search for new phenomena in events with an energetic jet and missing transverse momentum in pp collisions at $\sqrt{s} = 13$ TeV with the ATLAS detector,” *Phys. Rev. D* **103** no. 11, (2021) 112006, [arXiv:2102.10874 \[hep-ex\]](#).
- [13] **CMS** Collaboration, A. Tumasyan et al., “Search for new particles in events with energetic jets and large missing transverse momentum in proton-proton collisions at $\sqrt{s} = 13$ TeV,” [arXiv:2107.13021 \[hep-ex\]](#).
- [14] B. Holdom, “Two U(1)’s and Epsilon Charge Shifts,” *Phys. Lett. B* **166** (1986) 196–198.
- [15] M. Pospelov, A. Ritz, and M. B. Voloshin, “Secluded WIMP Dark Matter,” *Phys. Lett. B* **662** (2008) 53–61, [arXiv:0711.4866 \[hep-ph\]](#).
- [16] R. T. D’Agnolo and J. T. Ruderman, “Light Dark Matter from Forbidden Channels,” *Phys. Rev. Lett.* **115** no. 6, (2015) 061301, [arXiv:1505.07107 \[hep-ph\]](#).
- [17] J. M. Cline, H. Liu, T. Slatyer, and W. Xue, “Enabling Forbidden Dark Matter,” *Phys. Rev. D* **96** no. 8, (2017) 083521, [arXiv:1702.07716 \[hep-ph\]](#).
- [18] P. J. Fitzpatrick, H. Liu, T. R. Slatyer, and Y.-D. Tsai, “New Pathways to the Relic Abundance of Vector-Portal Dark Matter,” [arXiv:2011.01240 \[hep-ph\]](#).
- [19] C.-Y. Xing and S.-H. Zhu, “Dark Matter Freeze-Out via Catalyzed Annihilation,” *Phys. Rev. Lett.* **127** no. 6, (2021) 061101, [arXiv:2102.02447 \[hep-ph\]](#).
- [20] P. J. Fitzpatrick, H. Liu, T. R. Slatyer, and Y.-D. Tsai, “New Thermal Relic Targets for Inelastic Vector-Portal Dark Matter,” [arXiv:2105.05255 \[hep-ph\]](#).
- [21] M. Cirelli, P. Panci, K. Petraki, F. Sala, and M. Taoso, “Dark Matter’s secret liaisons: phenomenology of a dark U(1) sector with bound states,” *JCAP* **05** (2017) 036, [arXiv:1612.07295 \[hep-ph\]](#).
- [22] J. Liu, X.-P. Wang, and F. Yu, “A Tale of Two Portals: Testing Light, Hidden New Physics at Future e^+e^- Colliders,” *JHEP* **06** (2017) 077, [arXiv:1704.00730 \[hep-ph\]](#).
- [23] D. Tucker-Smith and N. Weiner, “Inelastic dark matter,” *Phys. Rev. D* **64** (2001) 043502, [arXiv:hep-ph/0101138](#).
- [24] S. Alekhin et al., “A facility to Search for Hidden Particles at the CERN SPS: the SHiP physics case,” *Rept. Prog. Phys.* **79** no. 12, (2016) 124201, [arXiv:1504.04855 \[hep-ph\]](#).
- [25] M. Battaglieri et al., “US Cosmic Visions: New Ideas in Dark Matter 2017: Community Report,” in *U.S. Cosmic Visions: New Ideas in Dark Matter*. 7, 2017. [arXiv:1707.04591 \[hep-ph\]](#).
- [26] **BDX** Collaboration, M. Battaglieri et al., “Dark matter search in a Beam-Dump eXperiment (BDX) at Jefferson Lab: an update on PR12-16-001,” [arXiv:1712.01518 \[physics.ins-det\]](#).
- [27] A. Berlin, N. Blinov, G. Krnjaic, P. Schuster, and N. Toro, “Dark Matter, Millicharges, Axion and Scalar Particles, Gauge Bosons, and Other New Physics with LDMX,” *Phys. Rev. D* **99** no. 7, (2019) 075001, [arXiv:1807.01730 \[hep-ph\]](#).
- [28] **LDMX** Collaboration, T. Åkesson et al., “Light Dark Matter eXperiment (LDMX),” [arXiv:1808.05219 \[hep-ex\]](#).
- [29] Y.-D. Tsai, P. deNiverville, and M. X. Liu, “Dark Photon and Muon $g - 2$ Inspired Inelastic Dark Matter Models at the High-Energy Intensity Frontier,” *Phys. Rev. Lett.* **126** no. 18, (2021) 181801, [arXiv:1908.07525 \[hep-ph\]](#).
- [30] T. R. Slatyer, “Indirect Dark Matter Signatures in the Cosmic Dark Ages II. Ionization, Heating and Photon Production from Arbitrary Energy Injections,” *Phys. Rev. D* **93** no. 2, (2016) 023521, [arXiv:1506.03812 \[astro-ph.CO\]](#).
- [31] T. Cohen, D. E. Morrissey, and A. Pierce, “Changes in Dark Matter Properties After Freeze-Out,” *Phys. Rev. D* **78** (2008) 111701, [arXiv:0808.3994 \[hep-ph\]](#).
- [32] M. J. Baker and J. Kopp, “Dark Matter Decay between Phase Transitions at the Weak Scale,” *Phys. Rev. Lett.* **119** no. 6, (2017) 061801, [arXiv:1608.07578 \[hep-ph\]](#).
- [33] A. Kobakhidze, M. A. Schmidt, and M. Talia, “Mechanism for dark matter depopulation,” *Phys. Rev. D* **98** no. 9, (2018) 095026, [arXiv:1712.05170 \[hep-ph\]](#).
- [34] M. J. Baker, M. Breitbach, J. Kopp, and L. Mittnacht, “Dynamic Freeze-In: Impact of Thermal Masses and Cosmological Phase Transitions on Dark Matter Production,” *JHEP* **03** (2018) 114, [arXiv:1712.03962 \[hep-ph\]](#).
- [35] M. J. Baker and L. Mittnacht, “Variations on the Vev Flip-Flop: Instantaneous Freeze-out and Decaying Dark

- Matter,” *JHEP* **05** (2019) 070, [arXiv:1811.03101 \[hep-ph\]](#).
- [36] A. Hektor, K. Kannike, and V. Vaskonen, “Modifying dark matter indirect detection signals by thermal effects at freeze-out,” *Phys. Rev. D* **98** no. 1, (2018) 015032, [arXiv:1801.06184 \[hep-ph\]](#).
- [37] L. Bian and Y.-L. Tang, “Thermally modified sterile neutrino portal dark matter and gravitational waves from phase transition: The Freeze-in case,” *JHEP* **12** (2018) 006, [arXiv:1810.03172 \[hep-ph\]](#).
- [38] L. Bian and X. Liu, “Two-step strongly first-order electroweak phase transition modified FIMP dark matter, gravitational wave signals, and the neutrino mass,” *Phys. Rev. D* **99** no. 5, (2019) 055003, [arXiv:1811.03279 \[hep-ph\]](#).
- [39] A. Kobakhidze, M. A. Schmidt, and M. Talia, “Thermal dark matter abundance under non-standard macroscopic conditions in the early universe,” *JCAP* **03** (2020) 059, [arXiv:1910.01433 \[hep-ph\]](#).
- [40] L. Heurtier and H. Partouche, “Spontaneous Freeze Out of Dark Matter From an Early Thermal Phase Transition,” *Phys. Rev. D* **101** no. 4, (2020) 043527, [arXiv:1912.02828 \[hep-ph\]](#).
- [41] L. Darmé, A. Hryczuk, D. Karamitros, and L. Roszkowski, “Forbidden frozen-in dark matter,” *JHEP* **11** (2019) 159, [arXiv:1908.05685 \[hep-ph\]](#).
- [42] H. Davoudiasl and G. Mohlabeng, “Getting a THUMP from a WIMP,” *JHEP* **04** (2020) 177, [arXiv:1912.05572 \[hep-ph\]](#).
- [43] V. De Romeri, D. Karamitros, O. Lebedev, and T. Toma, “Neutrino dark matter and the Higgs portal: improved freeze-in analysis,” *JHEP* **10** (2020) 137, [arXiv:2003.12606 \[hep-ph\]](#).
- [44] C. Jaramillo, M. Lindner, and W. Rodejohann, “Seesaw neutrino dark matter by freeze-out,” *JCAP* **04** (2021) 023, [arXiv:2004.12904 \[hep-ph\]](#).
- [45] K. Nakayama and W. Yin, “Hidden Photon and Axion Dark Matter from Symmetry Breaking,” [arXiv:2105.14549 \[hep-ph\]](#).
- [46] B. Batell and A. Ghalsasi, “Thermal Misalignment of Scalar Dark Matter,” [arXiv:2109.04476 \[hep-ph\]](#).
- [47] D. Croon, G. Elor, R. Houtz, H. Murayama, and G. White, “Light Dark Matter through Resonance Scanning,” [arXiv:2012.15284 \[hep-ph\]](#).
- [48] H. Davoudiasl, R. Kitano, G. D. Kribs, H. Murayama, and P. J. Steinhardt, “Gravitational baryogenesis,” *Phys. Rev. Lett.* **93** (2004) 201301, [arXiv:hep-ph/0403019](#).
- [49] R. R. Caldwell and S. S. Gubser, “Brief history of curvature,” *Phys. Rev. D* **87** no. 6, (2013) 063523, [arXiv:1302.1201 \[astro-ph.CO\]](#).
- [50] M. Dine, L. Randall, and S. D. Thomas, “Supersymmetry breaking in the early universe,” *Phys. Rev. Lett.* **75** (1995) 398–401, [arXiv:hep-ph/9503303](#).
- [51] M. Dine, L. Randall, and S. D. Thomas, “Baryogenesis from flat directions of the supersymmetric standard model,” *Nucl. Phys. B* **458** (1996) 291–326, [arXiv:hep-ph/9507453](#).
- [52] **BESIII** Collaboration, M. Ablikim et al., “Dark Photon Search in the Mass Range Between 1.5 and 3.4 GeV/ c^2 ,” *Phys. Lett. B* **774** (2017) 252–257, [arXiv:1705.04265 \[hep-ex\]](#).
- [53] **BaBar** Collaboration, J. P. Lees et al., “Search for Invisible Decays of a Dark Photon Produced in e^+e^- Collisions at BaBar,” *Phys. Rev. Lett.* **119** no. 13, (2017) 131804, [arXiv:1702.03327 \[hep-ex\]](#).
- [54] Y. Zhang, W.-T. Zhang, M. Song, X.-A. Pan, Z.-M. Niu, and G. Li, “Probing invisible decay of dark photon at BESIII and future STCF via monophoton searches,” *Phys. Rev. D* **100** no. 11, (2019) 115016, [arXiv:1907.07046 \[hep-ph\]](#).
- [55] **LHCb** Collaboration, R. Aaij et al., “Search for $A' \rightarrow \mu^+\mu^-$ Decays,” *Phys. Rev. Lett.* **124** no. 4, (2020) 041801, [arXiv:1910.06926 \[hep-ex\]](#).
- [56] **CMS** Collaboration, A. M. Sirunyan et al., “Search for a Narrow Resonance Lighter than 200 GeV Decaying to a Pair of Muons in Proton-Proton Collisions at $\sqrt{s} = \text{TeV}$,” *Phys. Rev. Lett.* **124** no. 13, (2020) 131802, [arXiv:1912.04776 \[hep-ex\]](#).
- [57] **ATLAS** Collaboration, G. Aad et al., “Search for high-mass dilepton resonances using 139 fb $^{-1}$ of pp collision data collected at $\sqrt{s} = 13$ TeV with the ATLAS detector,” *Phys. Lett. B* **796** (2019) 68–87, [arXiv:1903.06248 \[hep-ex\]](#).
- [58] **CMS** Collaboration, A. M. Sirunyan et al., “Search for resonant and nonresonant new phenomena in high-mass dilepton final states at $\sqrt{s} = 13$ TeV,” *JHEP* **07** (2021) 208, [arXiv:2103.02708 \[hep-ex\]](#).

APPENDIX

The annihilation cross-sections– We show the full expression for annihilation cross-sections, which are omitted in the main text. For the $A'\phi$ channel, the s -wave part of annihilation cross-section is

$$\begin{aligned} \langle\sigma v_{A'\phi}\rangle &\approx \sigma v_{A'\phi} = \frac{g_d^4 \left(-2(q^2 - 20)r^2 + (q^2 - 4)^2 + r^4 \right) \sqrt{q^4 - 2q^2(r^2 + 4) + (r^2 - 4)^2}}{256\pi m_\psi^2 (r^2 - 4)^2} \\ &\approx \frac{g_d^4}{256\pi m_\psi^2} \frac{r^4 + 40r^2 + 16}{|4 - r^2|} + \mathcal{O}(q^2), \end{aligned} \quad (21)$$

where $q \equiv m_\phi/m_\psi$ is a small parameter. Since the cross-section is s -wave dominant, we use the approximation $\langle\sigma v_{A'\phi}\rangle \approx \sigma v_{A'\phi}$, where the latter is the cross-section without thermally averaging. In the analytic calculation for DM yield, we have used the simpler form in the second line. While in the numeric calculation, we have used the expression in the first line. In the left panel of Fig. 4, we show the analytic results agree with the numeric calculation for both transient secluded channels. For $A'A'$, at small x the A' is massless thus the cross-section is flat. Near the threshold $x_{A'A'}$ (i.e. $m_{A'} = m_\psi$) both results drops but for different reasons. The analytic result decreases due to phase space, while numeric results also incorporate Boltzmann suppression beyond the threshold. For $A'\phi$, the analytic result becomes zero at threshold $x_{A'\phi}$, while the numeric result has a Boltzmann tail from thermally averaging. For $x < x_{A'A'}$, the $A'A'$ channel contribution dominates, while for $x > x_{A'\phi}$, the accidental resonant $A'\phi$ channel takes over. Both channels together provide the right relic abundance for the benchmark \blacktriangle .

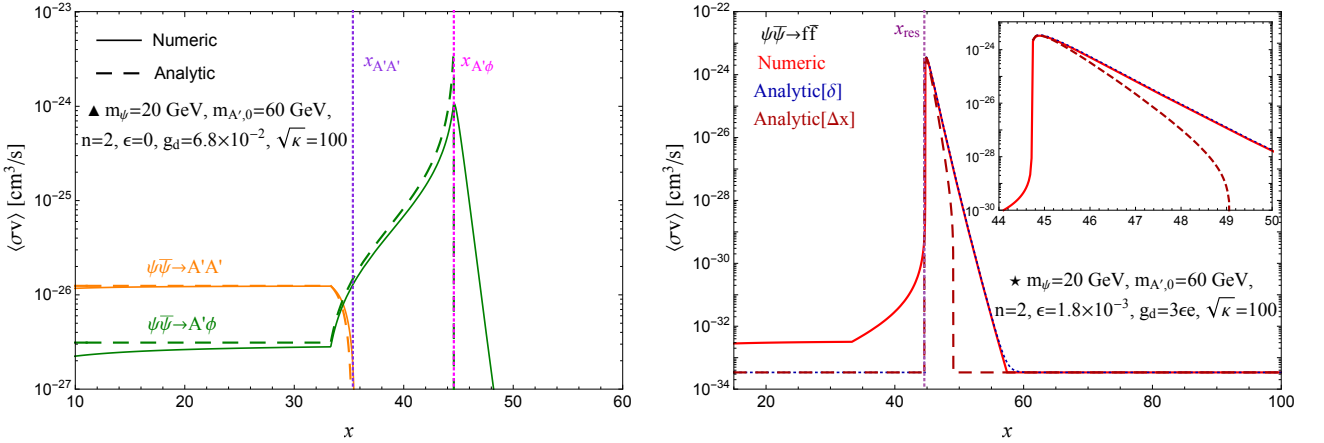


Figure 4. The $\langle\sigma v\rangle$ from analytic and numeric calculations for $A'A'$ and $A'\phi$ in the left panel and for resonant $f\bar{f}$ in the right panel, with $n = 2$. The benchmark \blacktriangle has a large g_d and works for transient secluded annihilation, while \blackstar has a small g_d and is for transient secluded annihilation. An inset figure is provided for the right panel near the threshold x_{res} .

For $f\bar{f}$ channel, the resonant annihilation cross-section in small Δx expansion with $x = x_{\text{res}} + \Delta x$ is

$$\sum_f \langle\sigma v\rangle_{f\bar{f}}^{\text{res}} \approx \frac{3\sqrt{n\pi\Delta x} g_d^2}{4m_\psi^2} e^{-\frac{n\Delta x}{4}(r_0^2-4)} (r_0^2 - 4)^{\frac{n-2}{2n}} \kappa^{1/n} \left(1 - \frac{3g_d^2\sqrt{n\Delta x}}{4n_{\text{dof}}\epsilon^2 e^2} (r_0^2 - 4)^{\frac{n+1}{2n}} \kappa^{\frac{-1}{2n}} \right), \quad (22)$$

where in the last term, if $g_d^2\sqrt{n\Delta x} \gtrsim n_{\text{dof}}\epsilon^2 e^2$ it will be invalid and return a negative result. We plot in analytic result in Eq. (22) and label it as “Analytic[Δx]” in the right panel of Fig. 4, which is a simplified form after Δx expansion. We compare it with the numeric result and the analytic result labeled as “Analytic[δ]” without the expansion. It is clear that the δ -function approximation for the resonance peak is quite successful. The simple analytic expression in Eq. (22) deviates from the other two at large Δx , but such simplification is necessary for the analytic relic abundance calculation. Near the resonance, the three results agree quite well with each other. Because the integration of $\langle\sigma v\rangle$ over x returns similar results, the simple expression can lead to a good match for relic abundance with the other two calculations.

The relic abundance yield– For relic abundance calculation, the relevant DM yield can be obtained by integrate over

$$Y^{-1} \approx \int_{x_{r_0}}^{x_{\text{th}}} dx \sqrt{\frac{\pi g_*}{45}} \frac{m_{\text{pl}} m_\psi}{x^2} \langle \sigma v \rangle, \quad (23)$$

where x_{th} are the thresholds for $A'A'$ and $A'\phi$ channels respectively and $g_*^{1/2}$ is assumed to be a constant. If the annihilation cross-section $\langle \sigma v \rangle$ is simple enough, one can obtain the indefinite integration functions, which are

$$F_{A'A'}(x, r_0, \kappa) = \left\{ \sqrt{r_0^2 - 2} \left(2(r_0^2 - 2) \operatorname{arctanh} \left[\sqrt{1 - \frac{(r_0^2 - 1)x^2}{\kappa}} \right] + \frac{\sqrt{\kappa(\kappa - (r_0^2 - 1)x^2)}}{\kappa - (r_0^2 - 2)x^2} \right) - (3r_0^2 - 5) \operatorname{arctan} \left[\sqrt{\frac{(r_0^2 - 2)(\kappa - (r_0^2 - 1)x^2)}{\kappa}} \right] \right\} \times \frac{-2}{\sqrt{\kappa}(r_0^2 - 2)^{3/2}}, \quad (24)$$

$$F_{A'\phi}(x, r_0, \kappa) = \frac{192}{\sqrt{(r_0^2 - 4)\kappa}} \operatorname{arctanh} \left(\frac{\sqrt{r_0^2 - 4}}{\sqrt{\kappa}} x \right) + \frac{r_0^2 + 44}{x} - \frac{\kappa}{3x^3}, \quad (25)$$

for $n = 2$, where we have assumed $g_*^{1/2}$ to be a constant. At the threshold $x_{A'A'}$ (i.e. $r = 1$), the function $F_{A'A'}$ becomes zero because the corresponding annihilation cross-section is proportional to high power in $1 - r$. For the $A'\phi$ channel, the function $F_{A'\phi}$ at threshold is non-zero. Plugging the indefinite integration functions, one can obtain the relic abundance yield in the main text.